ACS APPLIED MATERIALS & INTERFACES

Research Article

www.acsami.org

Superhydrophobic Surfaces Boost Fibril Self-Assembly of Amyloid β Peptides

Angelo Accardo,[*,†] Victoria Shalabaeva,[†] Emanuela Di Cola,[‡,§] Manfred Burghammer,[‡,⊥] Roman Krahne,[†] Christian Riekel,[‡] and Silvia Dante[†]

[†]Istituto Italiano di Tecnologia, Via Morego 30, Genova 16163, Italy

[‡]The European Synchrotron, CS40220, 38043 Cedex 9 Grenoble, France

[⊥]Department of Analytical Chemistry, Ghent University, Krijgslaan 281, Ghent 9000, Belgium

Supporting Information

ABSTRACT: Amyloid β (Aβ) peptides are the main constituents of Alzheimer's amyloid plaques in the brain. Here we report how the unique microfluidic flows exerted by droplets sitting on superhydrophobic surfaces can influence the aggregation mechanisms of several Aβ fragments by boosting their fibril self-assembly. Aβ(25−35), Aβ(1−40), and Aβ(12−28) were dried both on flat hydrophilic surfaces (contact angle (CA) = 37.3°) and on nanostructured superhydrophobic ones (CA = 175.8°). By embedding nanoroughened surfaces on top of highly X-ray transparent Si_3N_4 membranes, it was possible to probe the solid residues by raster-scan synchrotron radiation X-ray microdiffraction (μXRD). As compared to residues obtained on flat Si_3N_4 membranes, a general enhancement of fibrillar material was detected for all Aβ fragments dried on superhydrophobic surfaces, with a particular emphasis on the shorter ones. Indeed, both Aβ(25−35) and Aβ(12−28) showed a marked crystalline cross-β phase with varying fiber textures. The homogeneous evaporation rate provided by these nanostructured supports, and the possibility to use transparent membranes, can open a wide range of *in situ* X-ray and spectroscopic characterizations of amyloidal peptides involved in neurodegenerative diseases and for the fabrication of amyloid-based nanodevices.

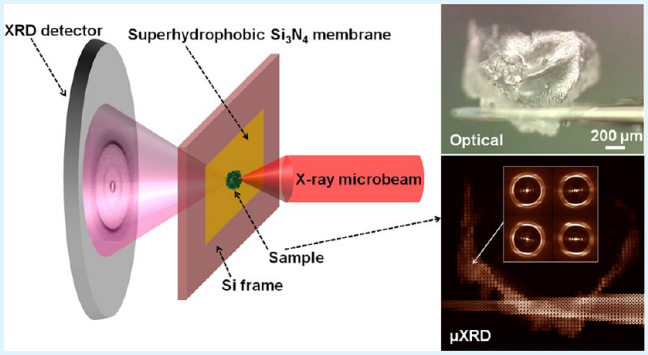

KEYWORDS: *superhydrophobic, convective flows, β-amyloid, fibril self-assembly, X-ray diffraction, synchrotron radiation*

INTRODUCTION

Amyloids are insoluble protein aggregates which are the main cause of more than 20 human diseases.[1,2] Among these amyloid-dependent syndromes are neurodegenerative pathologies such as Alzheimer's,[3] Parkinson's,[4] and Huntington's diseases[5] but also non-neuropathic localized amyloidosis such as diabetes mellitus type II.[6,7] Several approaches and innovative techniques have been used in recent decades to monitor the mechanisms which lead to the formation of the fibrils that are at the base of the previously mentioned diseases.[8−13] Considering that the number of patients affected by dementia will triple by 2050,[14] going from the actual 45 million to more than 135 million, the role of Alzheimer's disease (AD) assumes huge social implications. AD is characterized by the formation of extracellular amyloidal plaques, rich in fibrils of Aβ(1−40) and Aβ(1−42), which may act also as a reservoir for the most toxic Aβ membrane-soluble species, such as oligomers and protofibrils.[15,16] A more detailed knowledge of the aggregation path differentiation for the various Aβ species and of the final structure adopted by their fibers can add new information about the role of the different Aβs in the neurodegenerative mechanisms.

Our aim is to show that amyloid fibrillation mechanisms can be sensitively affected by the presence of superhydrophobic and superhydrophilic surfaces and materials.[17−20] Indeed, molecular self-assembly has been demonstrated for a wide range of materials and mechanisms of biological interest[17] such as synthetic amyloid peptides,[21,22] protein conformational changes,[18,23] biomineralization processes,[24] nanocrystallization,[25] DNA pulling,[26] and healthy/tumoral cell exosomes discrimination.[27] For droplets on hydrophilic surfaces, the evaporation rate is highest at the triple contact line resulting in an outward convective flow, while droplets on superhydrophobic surfaces (SHSs) have a more homogeneous evaporation rate across their surface resulting in the presence of a circulatory convective flow.[17] The flows generated inside evaporating drops on SHSs can then be used to induce ordering effects in the analyte as observed for the formation of fibrillar lysozyme related to a local convective flow field developed during pinning of the drying drop at the interface

Received: July 10, 2015
Accepted: August 26, 2015
Published: August 26, 2015

DOI: 10.1021/acsami.5b06219
ACS Appl. Mater. Interfaces 2015, 7, 20875−20884

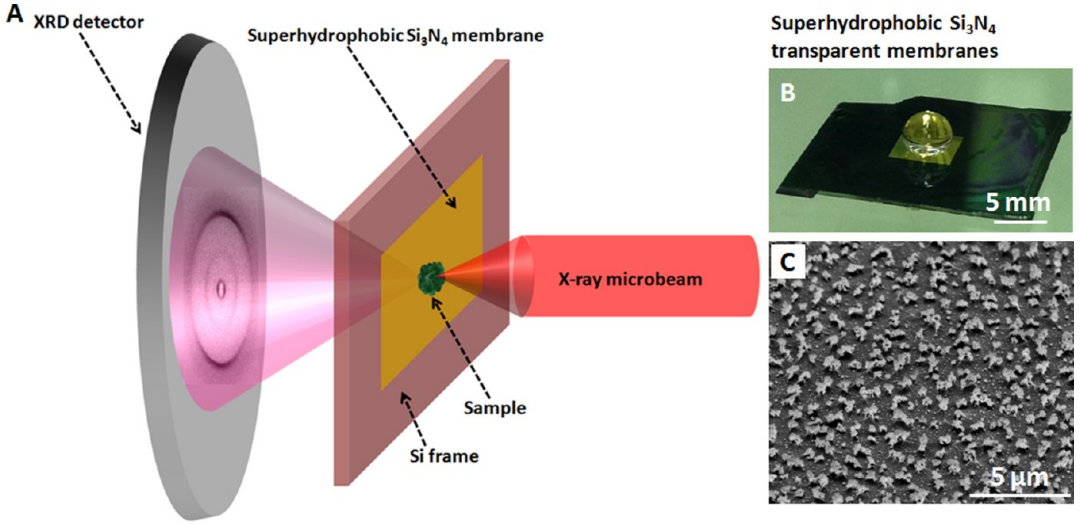

Figure 1. (A) Sketch of the experimental setup in the ID13 microfocus beamline with the X-ray beam impinging the sample formed over the superhydrophobic membrane and resulting in a scattering pattern recorded by the XRD detector (the experimental environment of the beamline is shown in SI Figure S1). (B) Aqueous droplet sitting on a superhydrophobic Si_3N_4 membrane. (C) SEM micrograph evidencing the rough morphology of the PMMA coating on the superhydrophobic Si_3N_4 membranes.

between the droplet and the substrate.[28] Further, synthetic trimeric to hexameric peptides show residues with marked cross-β sheet configuration after evaporation of quasi-contact-free droplets on superhydrophobic surfaces.[21,22] Under the same conditions, lysozyme in the presence of Ca^{2+} ions and a weakly acidic environment, self-assembles also into a fibrillar amyloidic phase on a time scale much shorter than that reported in literature.[23] On the other hand, several Aβ fragments, which are directly involved in the formation of AD plaques in the brain, show a direct correlation between secondary structure conformational changes, presence of nanostructured surfaces, and peptide concentration.[18,19] Besides amyloidal proteins involved in different pathologies, there is also a class of self-assembling peptides which, thanks to their low immunogenic and inflammatory potential, are at the center of a fascinating research branch that aims at different applications in the field of nanobiotechnology.[29,30] Among these "functional amyloids" are prion-related ones which are essential for the storage of memory in the brain,[31] amyloid fibers that serve as templates for the biosynthesis of melanin,[32,33] and amyloid fibrils employed as biomaterial for promoting cell adhesion, migration, and differentiation.[34] Considering all these aspects, the existence of a protocol able to control the formation of fibril self-assembly in such biocompounds would be crucial not just for better understanding the formation of amyloid material in neurodegenerative and non-neurodegenerative diseases but also for being exploited as a versatile fabrication approach of novel biomaterials for biomedicine and tissue engineering purposes.

The ability to manipulate biological soft matter aggregation has been exploited in this work to guide the process of fibril self-assembly in Aβ proteins by the peculiar microfluidic flows induced by biomimetic SHSs, which mimic the superhydrophobic features of lotus leaves. For this aim we embedded poly(methyl methacrylate) (PMMA) nanostructured SH coatings on ultrathin Si_3N_4 membranes in order to perform *in situ* X-ray microdiffraction (μXRD) studies on the dried residues. Following this approach we made a comparative evaluation of different amyloid β-peptides, namely, Aβ (25−35), Aβ (1−40), and Aβ (12−28), confined in droplet environments both on flat hydrophilic Si_3N_4 membranes and on SH ones. With the use of hydrophilic supports it is possible to observe characteristic ring-like moieties already reported elsewhere.[18,19,35] On the other hand, the homogeneous evaporation rate provided by superhydrophobic surfaces[17] induces the formation of free-standing samples. As compared to flat Si_3N_4 membranes, Aβ fragments in the presence of superhydrophobic supports result in a strong enhancement of the fibrillar component, often accompanied by a quasi-crystalline structure. We show that raster-scan diffraction with a micrometric synchrotron radiation X-ray beam is required for revealing local superstructures with variable fiber textures. The control over the aggregation mechanisms of fibril self-assembly in natural peptides, provided by the use of the protocol presented in this study, is both a valuable tool to shed more light on the processes resulting in the formation of amyloid fibrils in neurodegenerative diseases and a fabrication route for the development of amyloidal films to be used in the field of biomedicine. In this work, we present a new class of superhydrophobic X-ray transparent Si_3N_4 membranes, which allow to investigate the effects of convective flows in microliter droplets on the self-assembly mechanisms of amyloid-β peptides involved in Alzheimer's disease by μXRD.

EXPERIMENTAL SECTION

Aβ Peptides. Aβ(1−40) (H-Asp-Ala-Glu-Phe-Arg-His-Asp-Ser-Gly-Tyr-Glu-Val-His-His-Gln-Lys-Leu-Val-Phe-Phe-Ala-Glu-Asp-Val-Gly-Ser-Asn-Lys-Gly-Ala-Ile-Ile-Gly-Leu-Met-Val-Gly-Gly-Val-Val-OH; molecular formula, $C_{194}H_{295}N_{53}O_{58}S$), A$\beta$(12−28) (H-Val-His-His-Gln-Lys-Leu-Val-Phe-Phe-Ala-Glu-Asp-Val-Gly-Ser-Asn-Lys-OH; molecular formula, $C_{89}H_{135}N_{25}O_{25}$), and A$\beta$(25−35) (H-Gly-Ser-Asn-Lys-Gly-Ala-Ile-Ile-Gly-Leu-Met-OH; molecular formula, $C_{45}H_{81}N_{13}O_{14}S$) fragments were products of Bachem. The peptides were first dissolved in trifluoroacetic acid (TFA) at a concentration of 1 mg/mL to eliminate the presence of seeds and to obtain a monomeric peptide dispersion. TFA was dried under nitrogen, and the peptides were successively dissolved in Milli-Q water (1 mg/mL), shortly sonicated, and centrifuged at 10000 rpm for 10 min.

Superhydrophobic Si_3N_4 Membranes Fabrication. Si_3N_4−Si−Si_3N_4 ⟨100⟩ wafers (Si thickness, 525 μm; Si_3N_4 thickness, 500 nm) were purchased from University Wafer. We adopted an optical lithography process in order to obtain a matrix of single square Si_3N_4

DOI: 10.1021/acsami.5b06219
ACS Appl. Mater. Interfaces 2015, 7, 20875−20884

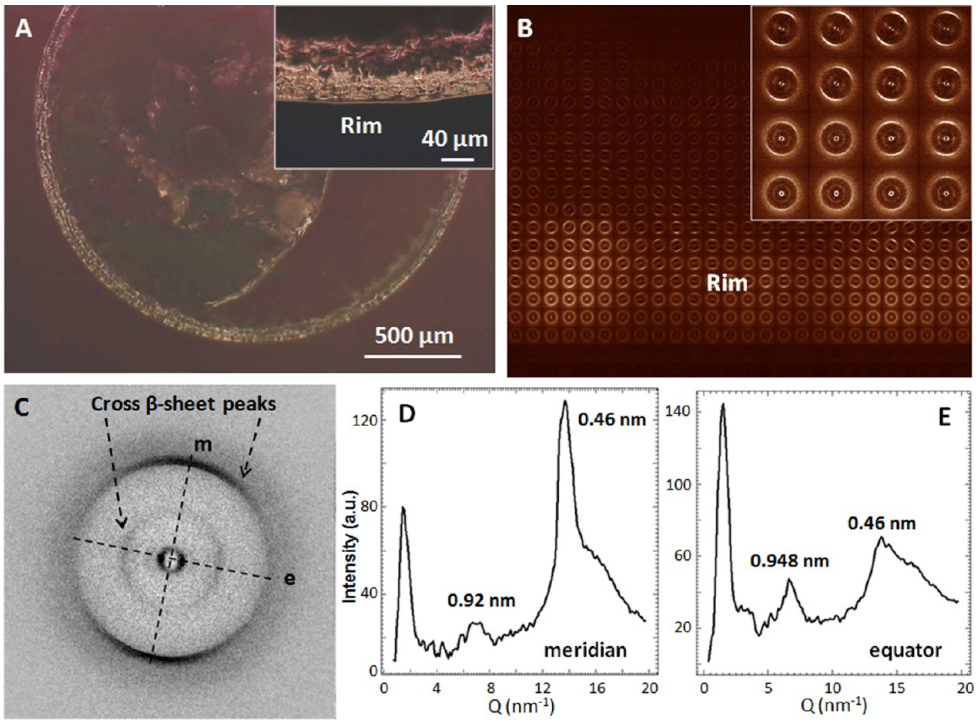

Figure 2. (A) Optical image of the Aβ(25−35) ring-like residue dried on a flat Si_3N_4 membrane (inset: close-up on the rim of the residue). (B) μXRD mesh scan of a portion of the rim in panel A (inset: close-up on a few μXRD patterns). (C) Typical orthogonal μXRD pattern from the rim of the residue highlighting the meridional and equatorial directions. (D, E) Azimuthal averages of the μXRD pattern of panel C along the meridian (D) and equatorial (E) directions.

membranes of 5 mm × 5 mm size. After spin-coating the wafer with S1813 positive resist at 4000 rpm for 60 s, the wafer went through a baking process (90 °C for 3 min). UV exposure was performed with a SUSS MicroTech mask-aligner in soft contact for 15 s, and it was followed by MF319 development for 1 min. A reactive ion etch process (Sentech 500 system; CHF_3, 70 cm^3(STP) min^{-1}; O_2, 5 cm^3(STP) min^{-1}; RF, 70 W; ICP, 200 W; P = 1 Pa) allowed etching of the Si_3N_4 regions not covered by the optical resist. The residual resist was then stripped by cold acetone (5 min), and the entire wafer passed through a wet etch based on KOH (100 g of KOH in 150 mL of H_2O at 105 °C) for 6−8 h. After etching the Si, the wafer was rinsed in Milli-Q water and baked at 65 °C to dry it completely before performing the superhydrophobic coating. The wafer was spin-coated with PMMA A11 (MicroChem) resist at 2000 rpm for 60 s and baked (180 °C for 30 min) obtaining an homogeneous layer of 1 μm thickness. A further plasma reactive ion etching process was employed to nanotexture the PMMA layer (ICP, 50 W; RF, 100 W; P = 6.5 Pa; O_2, 30 cm^3(STP) min^{-1}; 5 min) and to deposit a thin layer of Teflon on top of it (RF, 600 W; P = 3.6 Pa; C_4F_8, 85 cm^3(STP) min^{-1}; 5 s).

Contact Angle Measurements. The evaluation of the contact angle of aqueous droplets was estimated using a Kruss DSA100 setup, yielding a value of 37.3 ± 0.5° in the presence of flat pristine Si_3N_4 supports and 175.8 ± 0.5° in the presence of superhydrophobic Si_3N_4 supports (Supporting Information, Figure S1).

Synchrotron Radiation Experiments. μXRD experiments were performed at the ID13 Microfocus beamline of the European Synchrotron Radiation (ESRF). A monochromatic beam of λ = 0.0968633 nm was focused to a 2.5 (v) × 2.8 (h) μm^2 with about 3 × 10^{11} photons/s flux at the sample position using a transfocator[36] based on parabolic Be-refractive lenses. A Frelon CCD detector with 2048 × 2048 pixels of 50 × 50 μm^2 each (binned to 4 × 4) was used for data collection with an exposure of 0.5 s per pattern. The sample-to-detector distance was evaluated to be 142.1 mm by an Ag-behenate calibrant. Regions of interest of the sample were selected using an on-axis optical Olympus microscope aligned with the focal spot of the microbeam. The expression of the scattering vector Q in the illustrated azimuthal averages is equal to $Q = 4\pi \sin\theta/\lambda$, where θ is the diffraction angle and λ is the X-ray wavelength. FIT2D and an ID13 beamline in-house-developed software have been used for data analysis.

Scanning Electron Microscopy. Scanning electron microscopy (SEM) images were recorded by a FEI HELIOS Nanolab 600 instrument with a 10 kV acceleration voltage on samples sputtered with a 10 nm layer of gold.

RESULTS AND DISCUSSION

Figure 1A illustrates the typical experimental configuration of the μXRD experiments. After evaporation of 5 μL droplets of Aβ aqueous solutions (1 mg/mL) either on the super-hydrophobic Si_3N_4 membranes (Figure 1B,C) or on the flat pristine hydrophilic ones, the windows were mounted on a goniometer in front of a highly collimated X-ray beam to perform μXRD analysis (see Experimental Section, Figure 1A and Figure S1) in transmission geometry, exploiting the X-ray transparency of the membrane. In all the experiments that we performed, we evidenced a sharp difference between the residues obtained on superhydrophobic and hydrophilic supports. On the latter ones we obtained ring-like residues highly adherent to the surface (Figures 2A−4A) confirming how the evaporation flux configuration on a hydrophilic surface induces an outward convective flow, a pinning of the droplet, and the formation of a coffee-ring residue.[35] On the contrary, the presence of recirculating convective flows, of an extremely homogeneous evaporation rate, and of a low interaction between the droplet and the super-hydrorepellent surface[17] induced the formation of free-standing tridimensional residues (Figures 5A−7A).

μXRD Analysis of the Aβ Peptides Dried on Flat Si_3N_4 Membranes. Figure 2A shows the optical image of a typical ring-like residue obtained from Aβ(25−35) peptide dried on a flat Si_3N_4 membrane. The inset shows the morphology of the

DOI: 10.1021/acsami.5b06219
ACS Appl. Mater. Interfaces 2015, 7, 20875−20884

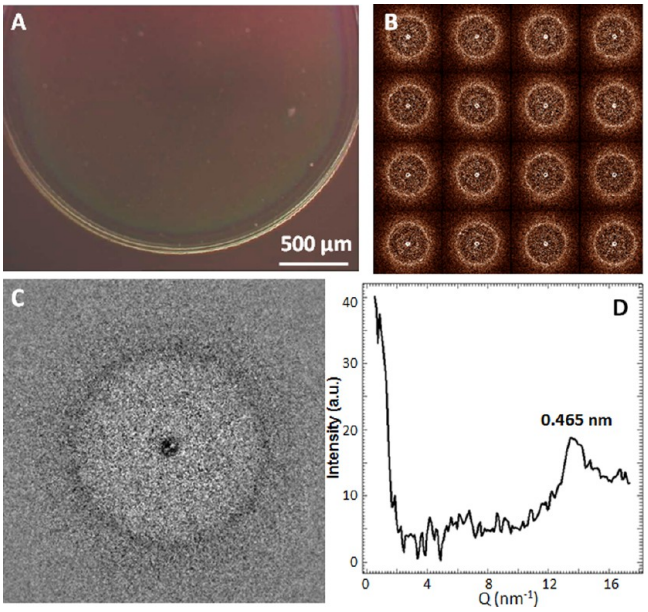

Figure 3. (A) Optical image of the Aβ(1−40) ring-like residue dried on a flat Si_3N_4 membrane. (B) μXRD mesh scan of a portion of the rim in panel A. (C) Typical μXRD pattern from the rim of the residue. (D) Azimuthal average of the μXRD pattern of panel C.

external rim while Figure 2B illustrates a XRD mesh scan of such a region where each single "pixel" is a XRD pattern resulting from a 2.5 (v) × 2.8 (h) μm^2 area according to the beam spot size (see Experimental Section).

This peptide has been extensively studied in previous works[18,19] on superhydrophilic surfaces where it showed a concentration-dependent α-helical to β-sheet transition. As shown by a typical XRD pattern of the rim (Figure 2C), in the presence of a conventional hydrophilic surface, such as flat Si_3N_4, we have the presence of a distinct cross-β sheet structure exhibiting a meridional d = 0.46 nm spacing (azimuthal average in Figure 2D), related to the distance between hydrogen-bonded strands, and an equatorial spacing of 0.948 nm (azimuthal average in Figure 2E), characteristic of β-sheet stacking. This configuration is universally recognized as the gold standard to unmistakably define amyloid fibrils.[2]

As demonstrated in previous works, the kinetics and amyloid morphology of Aβ peptides can be significantly different.[37] As further confirmation of these differences, Aβ(1−40) peptide showed a very different structure on flat supports if compared with the Aβ(25−35) one. Although the morphology of the residue looked very similar to the one of Aβ(25−35) (Figure 3A), the typical XRD patterns (Figure 3B,C) revealed only an unordered β-type phase with a weak contribution at $d \approx 0.465$ nm (Figure 3D), related to hydrogen-bonded strands. A similar configuration was found for the fragment Aβ(12−28) (Figure 4A−E), even though in this case we detected a quite sharp fibril orientation (Figure 4C). As shown by the XRD mesh scan and the single XRD pattern, respectively, in Figure 4B,C, the rim showed several areas with marked β-sheet conformation with a strongly oriented meridional reflection at $d \approx 0.472$ nm (Figure 4E). As happened for the Aβ(1−40) peptide, also in this case there was no appearance of the ≈1 nm reflection characteristic of β-sheet stacking, suggesting a possible stacking disorder.

It is worth noting that the aggregation kinetics of the investigated fragments, i.e., their conversion from non-amyloidogenic to amyloidogenic forms, differs significantly. In particular, for Aβ(1−40), which in aqueous solution, at

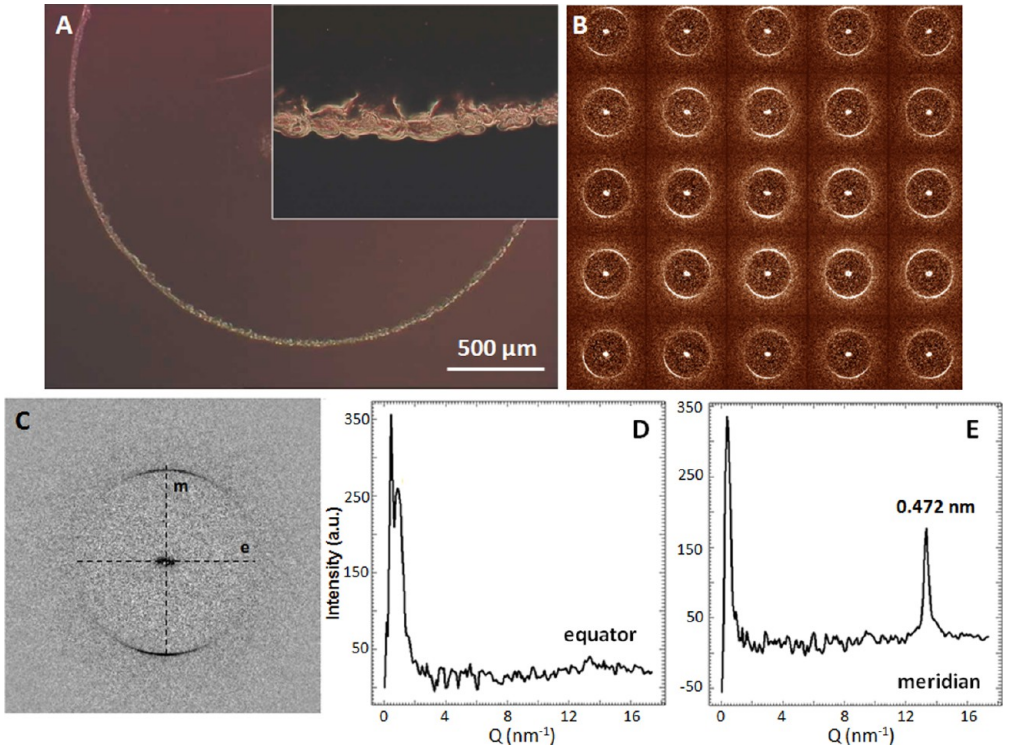

Figure 4. (A) Optical image of the Aβ(12−28) ring-like residue dried on a flat Si_3N_4 membrane (inset: close-up on the rim of the residue). (B) μXRD mesh scan of a portion of the rim in panel A. (C) Typical μXRD pattern from the rim of the residue highlighting the meridional and equatorial directions. (D, E) Azimuthal averages of the μXRD pattern of panel C along the equatorial (D) and meridian (E) directions.

DOI: 10.1021/acsami.5b06219
ACS Appl. Mater. Interfaces 2015, 7, 20875−20884

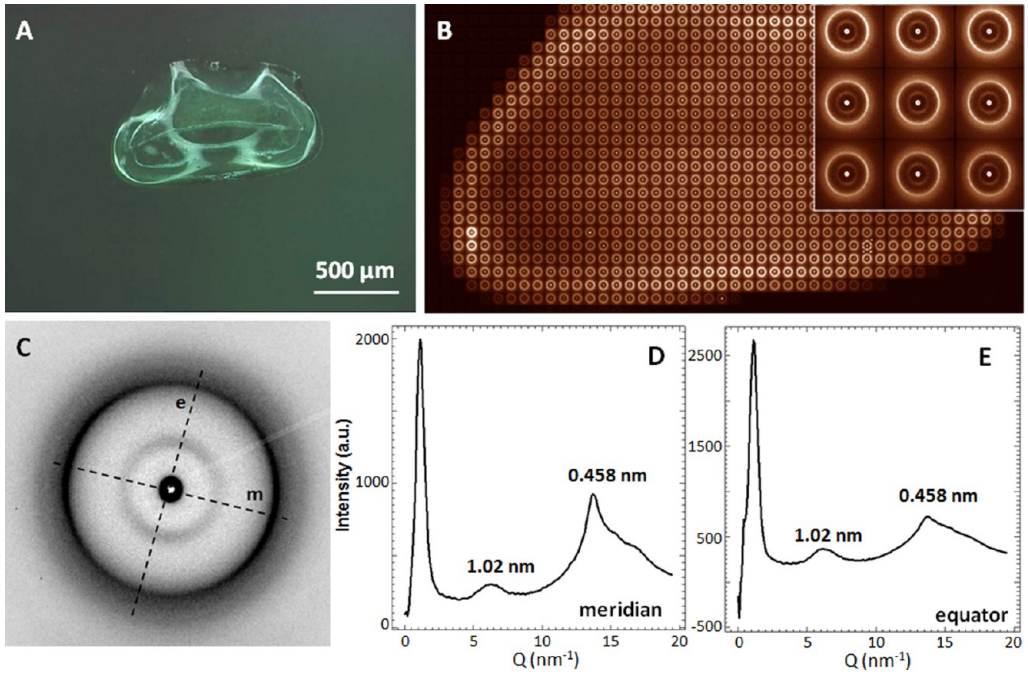

Figure 5. (A) Optical image of the Aβ(1−40) free-standing residue dried on a superhydrophobic Si_3N_4 membrane. (B) μXRD mesh scan of the residue in panel A (inset: close-up on a few μXRD patterns). (C) Typical μXRD pattern of the residue highlighting the meridian and equatorial directions. (D, E) Azimuthal averages of the μXRD pattern of panel C along the meridian (D) and equatorial (E) directions.

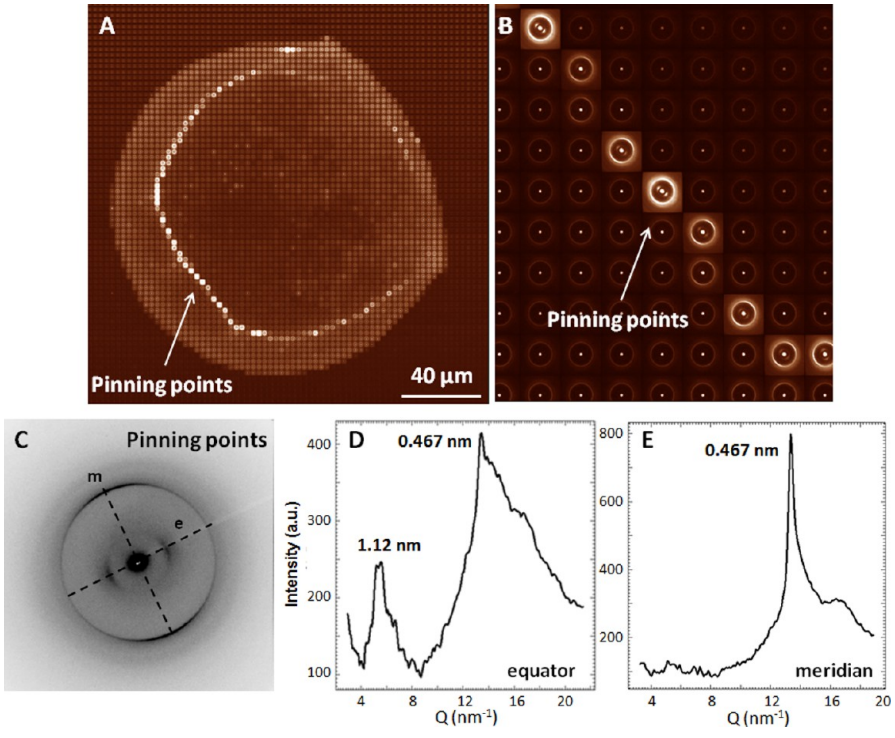

Figure 6. (A) μXRD mesh scan of the Aβ(12−28) residue dried on a superhydrophobic Si_3N_4 membrane. (B) Close-up on the μXRD patterns located in the proximity of the droplet pinning points. (C) Typical μXRD pattern of the residue highlighting the meridional and equatorial directions. (D, E) Azimuthal averages of the μXRD pattern of panel C along the equatorial (D) and meridian (E) directions.

physiological conditions, has a partially unfolded structure,[38] fibrillogenesis is rather low and may occur in several hours, depending on its concentration;[37,39] on the contrary the undecapeptide Aβ(25−35), which is the shorter Aβ fragment retaining the toxic characteristic of the full length Aβ peptide, shows a very rapid self-assembly behavior.[40] These differences reflect distinct aggregation paths and possibly the presence of different intermediates, which may therefore aggregate in diverse molecular architectures, as indicated by our findings.

μXRD Analysis of the Aβ Peptides Dried on Superhydrophobic Si_3N_4 Membranes. The conformation of the analyzed β-amyloid peptides changes abruptly in the presence

DOI: 10.1021/acsami.5b06219
ACS Appl. Mater. Interfaces 2015, 7, 20875−20884

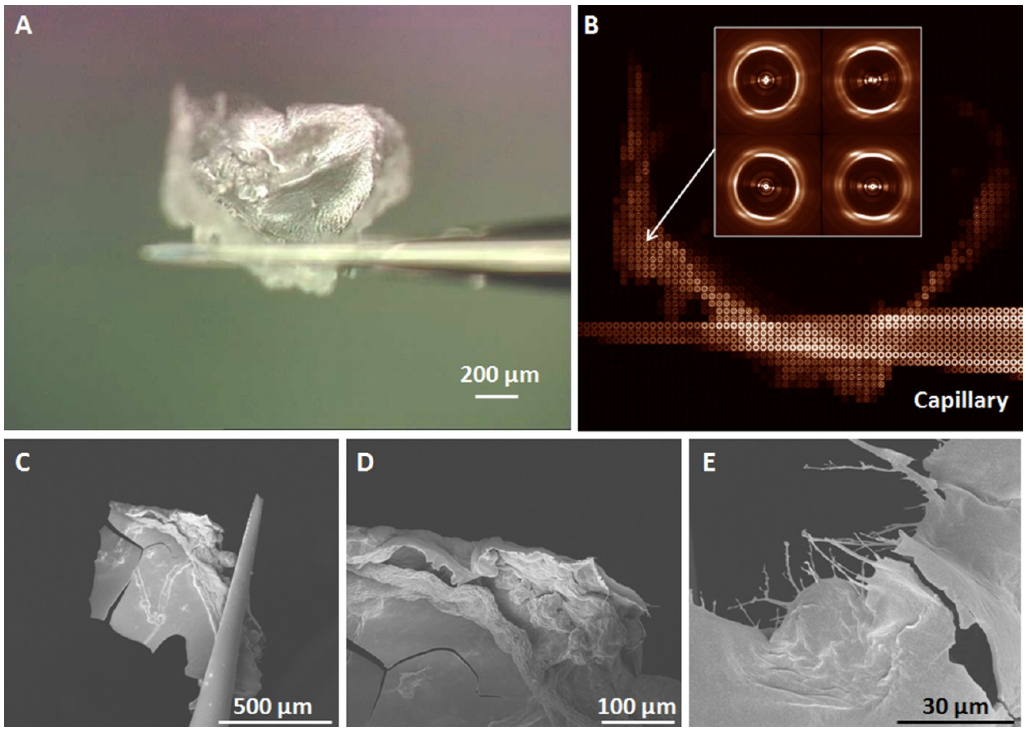

Figure 7. (A) Optical image of the Aβ(25−35) free-standing residue (attached to a glass capillary tip) dried on a superhydrophobic Si_3N_4 membrane. (B) μXRD mesh scan of the residue in panel A (inset: close-up on residue edge μXRD patterns). (C−E) SEM micrographs of the Aβ(25−35) residue in panel A.

of the superhydrophobic X-ray transparent supports. The optical image in Figure 5A shows a typical free-standing residue of a Aβ(1−40) solution droplet dried on the superhydrophobic surface. The μXRD raster-scan (Figure 5B) reveals a β-type fiber texture contrasting the weak unoriented powder-like β-type material obtained in the hydrophilic case (Figure 3). In particular the azimuthal averages along the equatorial and meridional directions (Figure 5D,E) of a typical XRD pattern (Figure 5C) extracted from the mesh scan, highlights the presence of an orthogonal cross-β-sheet configuration with the characteristic reflections at 1.02 and 0.458 nm. This result shows how, on very short time scales (each evaporation of a 5 μL droplet takes around 1 h), it is possible to boost the self-assembly of amyloid fibrils of an Aβ peptide which, if dried on conventional flat hydrophilic surfaces, does not show any ordered fibril structure. This can be attributed to the peculiar microfluidic flows and the homogeneous evaporation rate provided by droplets sitting on superhydrophobic supports that give enough time to the analyte to arrange in a gradual and more ordered way as compared with the hydrophilic substrate. In this latter case indeed the evaporation rate is very strong at the edge of the droplet and very low at the center, inducing a faster, but highly heterogeneous, evaporation rate which pushes the analyte to aggregate just at the rim of the solid residue.[18,19,35]

This "boosting" effect induced by SHSs becomes even more evident with the shorter peptides under investigation. Figure 6A shows a XRD mesh scan of the Aβ(12−28) peptide for which we obtained a free-standing residue characterized again by highly oriented amyloid fibril patterns as better shown in Figure 6B,C. Albeit in the presence of a hydrophilic support we already observed the presence of oriented patterns (Figure 4), in that case we could detect only the typical meridional reflection at $d \approx 0.472$ nm characteristic of hydrogen-bonded strands. On the contrary, in the superhydrophobic case it is possible to appreciate the presence of a very well defined region of the residue where the typical XRD patterns (Figure 6C) show a marked cross-β-sheet configuration including, besides the $d \approx 0.467$ nm reflection, also the orthogonal $d \approx 1.12$ nm one related to β-sheet stacking (Figure 6D,E).

The presence of these patterns mainly concentrated in a sort of "crown" is imputable to the pinning effect of the drying droplet, as reported in a previous investigation of our group.[17,28] Indeed, after being deposited in a superhydrophobic state (i.e., with a contact angle higher than 150°), during the evaporation process the droplet starts to shrink due to the volume reduction. According to the aspect ratio of the surface roughness (which sustains the droplet in a superhydrophobic state) and the viscosity of the droplet itself (which depends on the contained analyte, in this case Aβ peptide), before the end of the evaporation process the droplet dimension becomes so small that it starts to pin the asperities, thus transiting from a superhydrophobic "suspended" state (Cassie state) to a hydrophobic "pinned" one (Wenzel state).[17,28] In this configuration, the droplet is not anymore in a quasi-contact-free state on the substrate and this can provoke some sensitive changes in the convective flows acting inside the droplet and in a partial dis-homogenization of the evaporation rate. In summary, after having exploited the homogeneous evaporation rate of the superhydrophobic state for almost the whole drying process (the pinning effect on SHSs, such as the ones used here with a CA greater than 170°, happens only at the very end of the process), the ordered fibril material which formed during this time can get trapped in the proximity of the pinning points (Figure 6A,B) and form the crown illustrated by the XRD mesh scan.

Finally, the apex of fibril boosting induced by the superhydrophobic membranes was reached by Aβ(25−35).

DOI: 10.1021/acsami.5b06219
ACS Appl. Mater. Interfaces 2015, 7, 20875−20884

Already in its ring-like residue conformation, obtained with hydrophilic supports, this fragment showed a peculiar predisposition to form amyloid fibers as illustrated in Figure 2. We managed separating a free-standing residue from the superhydrophobic membrane and attached it to a glass capillary for X-ray analysis (Figure 7A). A composite raster-scan image reveals that the rim of the residue is characterized by highly oriented fiber diffraction patterns (Figure 7B). A highly structured fibrillar morphology can also be seen in scanning electron microscopy (SEM) images (Figure 7C–E). This contrasts powder-like patterns obtained by drying solubilized Aβ(25–35).[41]

The relatively large number of reflections exhibited by this Aβ fragment shows a para-crystalline order similar to the one detected also for other synthetic peptides[42] after 1 week incubation time, a far longer duration if compared with our droplet evaporation protocol of about 1 h.

A particularly well ordered XRD pattern coming from the outer rim of the free-standing residue reveals an orthogonal cross-β-structure with a number of equatorial peaks (Figure 8A). The a-axis is chosen along the meridional direction of the cross-β-peak and the b/c axes along the equatorial direction.[43] The reflection on the meridian with d = 0.473 nm is indexed as (100) and the peak at d = 0.239 nm as (200), suggesting parallel β-strands (Table 1).[19,44] The intensity profile of the cross-β-peak can be separated into three h0l reflections, the (110) reflection and a short-range-order peak revealing a semicrystalline material (Figure 8B,C). The short-range-order scattering ($d \sim 0.40$ nm) appears to be random. Some of the patterns in the raster-scan show only short-range-order scattering due to the absence of a crystalline fraction (not shown). Subtracting such a pattern from a semicrystalline one was used to enhance the visibility of the weak equatorial peaks. The d-spacing list and the deduced unit cell are collected in Table 1.

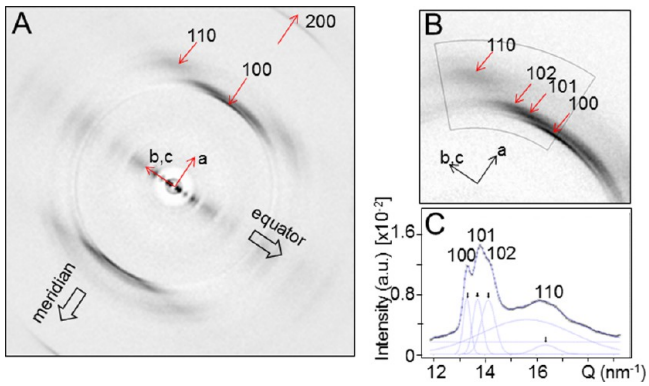

Figure 8. (A) XRD pattern of the Aβ(25–35) residue from the outer rim of the residue (Figure 7B). The reflections are indexed by an orthogonal cross-β structure. (B) Zoom into the cross-β-peak revealing a substructure due to h0l reflections and the neighboring (110) reflection. (C) Radial intensity profile corresponding to the azimuthally integrated sector in panel B. Four Gaussian profiles fitted the h0l and (110) peaks (black arrows), a broad Gaussian for short-range order, and a zero-order Lorentzian background. The fitted peaks and the resulting curve are in blue.

Table 1. Aβ(25-35) Crystallographic Parameters Based on an Orthogonal Cross-β Structure[a]

hkl	d (nm)	L (nm)	unit cell params ($\alpha = \beta = \gamma = 90°$)
(100)	0.473	25	a = 0.476 nm
(200)	0.239	14	b = 0.658 nm
(101)	0.458	16	c = 1.833 nm
(102)	0.445	13	
(110)	0.384	7	

[a]The particle size—L—was derived from the radial peak width of fitted Gaussian functions by Scherrer's equation.[49].

The unit cell of ~ 0.66 nm along the b-axis is shorter than expected for antiparallel β-sheets (~0.70 nm) supporting parallel β-sheets. The equatorial peaks extending to low angles suggest scattering due to amyloidal nanofilaments which has been studied extensively for other self-assembled oligopeptides and Aβ fragments.[45−47]

The positions of the individual peaks were determined by fitting Gaussian profiles (not shown). The orders n = 1–6 show a linear Q-dependence with a slope of 0.91 nm^{-1} (σ = 0.02; Figure 9A). For orders $n \geq 7$ we observe a deviation from a linear dependence which is probably due to 0kl equatorial reflections from the cross-β-structure (Figure 9A).

The equatorial intensity trace can be modeled by a cylinder with the 6.9 nm (σ = 0.1) diameter derived from the slope of the order plot (Figure 9; Supporting Information).[45,47] Other models based on solid, double-walled cylinders or β-sheet slabs did not match the cylinder diameter or provided less good fits.[46] The significant difference of the calculated and observed intensities at the position of the first order is attributed to a coincidence of the first-order interference peak of a hexagonal lattice of close-packed cylinders[48] with the form factor of the cylinder (Figure 9B). The decrease of the apparent particle size (L), derived from the peak broadenings by Scherrer's equation,[49] of L = 38 nm for the (100) reflection descending to 5–10 nm for the higher order reflections supports a loss of coherence for the higher order terms.

A less ordered equatorial trace is observed for several weaker patterns in the inner part of the residue corresponding to a period of about 4.3 nm. The peaks show a larger azimuthal spread, and the larger peak width suggests smaller domains than for the more ordered equatorial trace. A possible origin of this structural feature could be a partial melting of β-sheet strands as predicted by molecular dynamics (MD) simulations.[50] The comparable weaker equatorial features suggest, however, that this could only affect a small volume fraction while extensive loss of β-sheet structure occurs at 309 K according to MD simulations.[50] It might therefore be interesting to probe the thermal behavior of amyloid residues by combined nanocalorimetry and nanodiffraction[51] in the future.

CONCLUSIONS

In this work we showed how the presence of superhydrophobic surfaces can sensibly influence the aggregation mechanisms of Aβ peptides involved in the formation of fibroidal plaques at the origin of Alzheimer's disease.[3,15,16] In order to determine the structural configuration of the peptides under investigation by synchrotron μXRD techniques, we fabricated novel X-ray transparent superhydrophobic Si_3N_4 membranes. Our findings show how the comparison between the solid residues consisting of several Aβ peptides, namely, Aβ(1–40), Aβ(12–28), and Aβ(25–35), highlights peculiar conformational differences in the presence of a hydrophilic or superhydrophobic support. We observe a general enhancement of the fibril self-assembly

DOI: 10.1021/acsami.5b06219
ACS Appl. Mater. Interfaces 2015, 7, 20875–20884

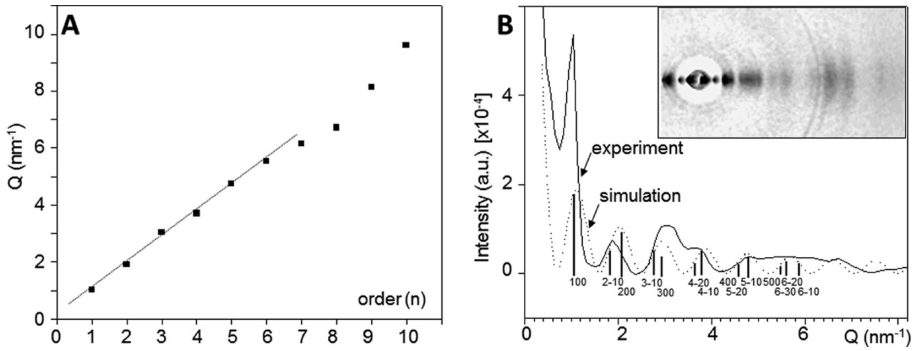

Figure 9. (A) Plot of position of low-angle orders against the order number. A linear regression curve with a slope of 0.91 nm^{-1} (σ = 0.02) has been fitted to the first six orders. (B) Experimental intensity profile of equatorial scattering (solid line) derived by azimuthal integration across the peaks shown in the inset. Random short-range-order scattering at the position of the β-peak has been subtracted in order to enhance the visibility of the peaks. The simulated scattering of a tube is shown as a dotted line. The vertical bars correspond to a hexagonal lattice of close-packed tubes.[45] Only one of each set of symmetry-related reflections is shown.

processes due to recirculating microfluidic flows and homogeneous evaporation rate provided by super-hydrorepellent surfaces.[17,52] The quasi-contact-free nature of the drying droplets allows the formation of free-standing residues, which are homogeneously characterized by an extended fibrillar structure in contrast to one of the ring-like substrate-adherent moieties obtained in hydrophilic conditions. Aβ(25−35) is particularly predisposed to form fiber textured structures which resulted in quasi-crystalline conformation over the SH Si_3N_4 membrane. The protocol that we used is a simple and straightforward method to monitor structural changes that can happen in amyloidal proteins. For this reason we envisage the extension of such study to biocompounds involved in other neurodegenerative diseases (e.g., α-synuclein/Parkinson's,[4] huntingtin/Huntington's[5]) and non-neurodegenerative ones (e.g., amylin/diabetes mellitus type II[6,7]). Further, the use of micro- and nanostructured supports to manipulate amyloidal soft matter could be also exploited as a smart fabrication protocol for the rapid realization of amyloidal fibers, which find application in tissue engineering, cell adhesion,[29,30,34,53] and other materials applications.[54−56]

■ ASSOCIATED CONTENT

Supporting Information

The Supporting Information is available free of charge on the ACS Publications website at DOI: 10.1021/acsami.5b06219.

Additional information on the simulation of equatorial X-ray scattering, the experimental setup, and the membranes related contact angles (PDF)

■ AUTHOR INFORMATION

Corresponding Author

*E-mail: angelo.accardo@iit.it. Tel.: +3901071781847.

Present Address

[§]Laboratoire Interdisciplinaire de Physique (LIPhy UMR5588 CNRS/UJF), 140 rue de la Physique, BP87 38402 Saint Martin d'Hères Cedex, France.

Notes

The authors declare no competing financial interest.

■ ACKNOWLEDGMENTS

The European Synchrotron Radiation Facility (ESRF) is thanked for granting beamtime (Proposal No. SC3843).

■ ABBREVIATIONS

AD, Alzheimer's disease
Aβ, amyloid beta
CA, contact angle
MD, molecular dynamics
PMMA, poly(methyl methacrylate)
SEM, scanning electron microscopy
SHS, superhydrophobic surface
TFA, trifluoroacetic acid
μXRD, X-ray microdiffraction

■ REFERENCES

(1) Serpell, L. C.; Sunde, M.; Blake, C. C. The Molecular Basis of Amyloidosis. *Cell. Mol. Life Sci.* **1997**, *53*, 871−887.

(2) Rambaran, R. N.; Serpell, L. C. Amyloid Fibrils: Abnormal Protein Assembly. *Prion* **2008**, *2*, 112−117.

(3) Koo, E. H.; Lansbury, P. T., Jr.; Kelly, J. W. Amyloid Diseases: Abnormal Protein Aggregation in Neurodegeneration. *Proc. Natl. Acad. Sci. U. S. A.* **1999**, *96*, 9989−9990.

(4) Irwin, D. J.; Lee, V. M.; Trojanowski, J. Q. Parkinson's Disease Dementia: Convergence of α-synuclein, Tau and Amyloid-β Pathologies. *Nat. Rev. Neurosci.* **2013**, *14*, 626−636.

(5) McGowan, D. P.; van Roon-Mom, W.; Holloway, H.; Bates, G. P.; Mangiarini, L.; Cooper, G. J.; Faull, R. L.; Snell, R. G. Amyloid-like Inclusions in Huntington's Disease. *Neuroscience* **2000**, *100*, 677−680.

(6) Westermark, P.; Andersson, A.; Westermark, G. T. Islet Amyloid Polypeptide, Islet Amyloid, and Diabetes Mellitus. *Physiol. Rev.* **2011**, *91*, 795−826.

(7) Höppener, J. W.; Lips, C. J. Role of Islet Amyloid in Type 2 Diabetes Mellitus. *Int. J. Biochem. Cell Biol.* **2006**, *38*, 726−736.

(8) Lee, J. S.; Um, E.; Park, J. K.; Park, C. B. Microfluidic Self-assembly of Insulin Monomers into Amyloid Fibrils on a Solid Surface. *Langmuir* **2008**, *24*, 7068−7071.

(9) Choi, Y. J.; Chae, S.; Kim, J. H.; Barald, K. F.; Park, J. Y.; Lee, S. H. Neurotoxic Amyloid Beta Oligomeric Assemblies Recreated in Microfluidic Platform with Interstitial Level of Slow Flow. *Sci. Rep.* **2013**, *3*, 1921.

(10) Seidi, A.; Kaji, H.; Annabi, N.; Ostrovidov, S.; Ramalingam, M.; Khademhosseini, A. A Microfluidic-Based Neurotoxin Concentration Gradient for the Generation of an *in Vitro* Model of Parkinson's Disease. *Biomicrofluidics* **2011**, *5*, 022214.

(11) Knowles, T. P. J.; White, D. A.; Abate, A. R.; Agresti, J. J.; Cohen, S. I. A.; Sperling, R. A.; De Genst, E. J.; Dobson, C. M.; Weitz, D. A. Observation of Spatial Propagation of Amyloid Assembly from Single Nuclei. *Proc. Natl. Acad. Sci. U. S. A.* **2011**, *108*, 14746−14751.

(12) Brancolini, G.; Corazza, A.; Vuano, M.; Fogolari, F.; Mimmi, M. C.; Bellotti, V.; Stoppini, M.; Corni, S.; Esposito, G. Probing the

DOI: 10.1021/acsami.5b06219
ACS Appl. Mater. Interfaces 2015, 7, 20875−20884

Influence of Citrate-Capped Gold Nanoparticles on an Amyloidogenic Protein. *ACS Nano* **2015**, *9*, 2600−2613.
(13) Chou, I. H.; Benford, M.; Beier, H. T.; Coté, G. L.; Wang, M.; Jing, N.; Kameoka, J.; Good, T. A. Nanofluidic Biosensing for Beta-amyloid Detection Using Surface Enhanced Raman Spectroscopy. *Nano Lett.* **2008**, *8*, 1729−1735.
(14) http://www.alz.co.uk/.
(15) Mucke, L.; Selkoe, D. J. Neurotoxicity of Amyloid β-Protein: Synaptic and Network Dysfunction. *Cold Spring Harbor Perspect. Med.* **2012**, *2*, a006338.
(16) Walsh, D. M.; Klyubin, I.; Fadeeva, J. V.; Cullen, W. K.; Anwyl, R.; Wolfe, S.; Rowan, M. J.; Selkoe, D. J. Naturally Secreted Oligomers of Amyloid Beta Protein Potently Inhibit Hippocampal Long-term Potentiation in vivo. *Nature* **2002**, *416*, 535−539.
(17) Accardo, A.; Di Fabrizio, E.; Limongi, T.; Marinaro, G.; Riekel, C. Probing Droplets on Superhydrophobic Surfaces by Synchrotron Radiation Scattering Techniques. *J. Synchrotron Radiat.* **2014**, *21*, 643−653.
(18) Accardo, A.; Shalabaeva, V.; Cotte, M.; Burghammer, M.; Krahne, R.; Riekel, C.; Dante, S. Amyloid β Peptide Conformational Changes in the Presence of a Lipid Membrane System. *Langmuir* **2014**, *30*, 3191−3198.
(19) Accardo, A.; Shalabaeva, V.; Hesse, B.; Cotte, M.; Krahne, R.; Riekel, C.; Dante, S. Synchrotron m-FTIR highlights amyloid-b conformational changes under the effect of surface wettability and external agents. *Vib. Spectrosc.* **2015**, *80*, 30−35.
(20) Pronchik, J.; He, X.; Giurleo, J. T.; Talaga, D. S. In Vitro Formation of Amyloid from Alpha-Synuclein Is Dominated by Reactions at Hydrophobic Interfaces. *J. Am. Chem. Soc.* **2010**, *132*, 9797−9803.
(21) Hauser, C. A.; Deng, R.; Mishra, A.; Loo, Y.; Khoe, U.; Zhuang, F.; Cheong, D. W.; Accardo, A.; Sullivan, M. B.; Riekel, C.; Ying, J. Y.; Hauser, U. A. Natural Tri- to Hexapeptides Self-assemble in Water to Amyloid Beta-type Fiber Aggregates by Unexpected Alpha-helical Intermediate Structures. *Proc. Natl. Acad. Sci. U. S. A.* **2011**, *108*, 1361−1366.
(22) Lakshmanan, A.; Cheong, D. W.; Accardo, A.; Di Fabrizio, E.; Riekel, C.; Hauser, C. A. Aliphatic Peptides Show Similar Self-assembly to Amyloid Core Sequences, Challenging the Importance of Aromatic Interactions in Amyloidosis. *Proc. Natl. Acad. Sci. U. S. A.* **2013**, *110*, 519−524.
(23) Accardo, A.; Burghammer, M.; Di Cola, E.; Reynolds, M.; Di Fabrizio, E.; Riekel, C. Lysozyme Fibrillation Induced by Convective Flow Under Quasi Contact-free Conditions. *Soft Matter* **2011**, *7*, 6792−6796.
(24) Accardo, A.; Mecarini, F.; Leoncini, M.; Brandi, F.; Di Cola, E.; Burghammer, M.; Riekel, C.; Di Fabrizio, E. Fast, Active Droplet Interaction: Coalescence and Reactive Mixing Controlled by Electrowetting on a Superhydrophobic Surface. *Lab Chip* **2013**, *13*, 332−335.
(25) Marinaro, G.; Accardo, A.; De Angelis, F.; Dane, T.; Weinhausen, B.; Burghammer, M.; Riekel, C. A Superhydrophobic Chip Based on SU-8 Photoresist Pillars Suspended on a Silicon Nitride Membrane. *Lab Chip* **2014**, *14*, 3705−3709.
(26) Miele, E.; Accardo, A.; Falqui, A.; Marini, M.; Giugni, A.; Leoncini, M.; De Angelis, F.; Krahne, R.; Di Fabrizio, E. Writing and Functionalisation of Suspended DNA Nanowires on Superhydrophobic Pillar Arrays. *Small* **2015**, *11*, 134−140.
(27) Accardo, A.; Tirinato, L.; Altamura, D.; Sibillano, T.; Giannini, C.; Riekel, C.; Di Fabrizio, E. Superhydrophobic Surfaces Allow Probing of Exosome Self Organization Using X-ray Scattering. *Nanoscale* **2013**, *5*, 2295−2299.
(28) Accardo, A.; Gentile, F.; Mecarini, F.; De Angelis, F.; Burghammer, M.; Di Fabrizio, E.; Riekel, C. In Situ X-ray Scattering Studies of Protein Solution Droplets Drying on Micro- and Nanopatterned Superhydrophobic PMMA Surfaces. *Langmuir* **2010**, *26*, 15057−15064.
(29) Hauser, C. A.; Zhang, S. Designer Self-assembling Peptide Nanofiber Biological Materials. *Chem. Soc. Rev.* **2010**, *39*, 2780−2790.
(30) Hauser, C. A.; Maurer-Stroh, S.; Martins, I. C. Amyloid-based Nanosensors and Nanodevices. *Chem. Soc. Rev.* **2014**, *43*, 5326−5345.
(31) Shorter, J.; Lindquist, S. Prions as Adaptive Conduits of Memory and Inheritance. *Nat. Rev. Genet.* **2005**, *6*, 435−450.
(32) Hu, K. N.; McGlinchey, R. P.; Wickner, R. B.; Tycko, R. Segmental Polymorphism in a Functional Amyloid. *Biophys. J.* **2011**, *101*, 2242−2250.
(33) Rochin, L.; Hurbain, I.; Serneels, L.; Fort, C.; Watt, B.; Leblanc, P.; Marks, M. S.; De Strooper, B.; Raposo, G.; van Niel, G. BACE2 Processes PMEL to Form the Melanosome Amyloid Matrix in Pigment Cells. *Proc. Natl. Acad. Sci. U. S. A.* **2013**, *110*, 10658−10663.
(34) Gras, S. L.; Tickler, A. K.; Squires, A. M.; Devlin, G. L.; Horton, M. A.; Dobson, C. M.; MacPhee, C. E. Functionalised Amyloid Fibrils for Roles in Cell Adhesion. *Biomaterials* **2008**, *29*, 1553−1562.
(35) Deegan, R. D.; Bakajin, O.; Dupont, T. F.; Huber, G.; Nagel, S. R.; Witten, T. A. Capillary Flow as the Cause of Ring Stains from Dried Liquid Drops. *Nature* **1997**, *389*, 827−829.
(36) Vaughan, G. B. M.; Wright, J. P.; Bytchkov, A.; Rossat, M.; Gleyzolle, H.; Snigireva, I.; Snigirev, A. X-ray Transfocators: Focusing Devices Based on Compound Refractive Lenses. *J. Synchrotron Radiat.* **2011**, *18*, 125−133.
(37) Kuperstein, I.; Broersen, K.; Benilova, I.; Rozenski, J.; Jonckheere, W.; Debulpaep, M.; Vandersteen, A.; Segers-Nolten, I.; Van Der Werf, K.; Subramaniam, V.; Braeken, D.; Callewaert, G.; Bartic, C.; D'Hooge, R.; Martins, I. C.; Rousseau, F.; Schymkowitz, J.; De Strooper, B. Neurotoxicity of Alzheimer's Disease Aβ Peptides Is Induced by Small Changes in the Aβ42 to Aβ40 Ratio. *EMBO J.* **2010**, *29*, 3408−3420.
(38) Vivekanandan, S.; Brender, J. R.; Lee, S. Y.; Ramamoorthy, A. A Partially Folded Structure of Amyloid-Beta(1−40) in an Aqueous Environment. *Biochem. Biophys. Res. Commun.* **2011**, *411*, 312−316.
(39) Canale, C.; Seghezza, S.; Vilasi, S.; Carrotta, R.; Bulone, D.; Diaspro, A.; San Biagio, P. L.; Dante, S. Different Effects of Alzheimer's Peptide Aβ(1−40) Oligomers and Fibrils on Supported Lipid Membranes. *Biophys. Chem.* **2013**, *182*, 23−29.
(40) Millucci, L.; Raggiaschi, R.; Franceschini, D.; Terstappen, G.; Santucci, A. Rapid Aggregation and Assembly in Aqueous Solution of Aβ (25−35) Peptide. *J. Biosci.* **2009**, *34*, 293−303.
(41) Bond, J. P.; Deverin, S. P.; Inouye, H.; El-Agnaf, O. M. A.; Teeter, M. M.; Kirschner, D. A. Assemblies of Alzheimer's Peptides Aβ25−35 and Aβ31−35: Reverse-Turn Conformation and Side Chain Interactions Revealed by X-Ray Diffraction. *J. Struct. Biol.* **2003**, *141*, 156−170.
(42) Morris, K. L.; Rodger, A.; Hicks, M. R.; Debulpaep, M.; Schymkowitz, J.; Rousseau, F.; Serpell, L. C. Exploring the Sequence−structure Relationship for Amyloid Peptides. *Biochem. J.* **2013**, *450*, 275−283.
(43) Weisman, S.; Okada, S.; Mudie, S. T.; Huson, M. C.; Trueman, H. E.; Sriskantha, A.; Haritos, V. S.; Sutherland, T. D. Fifty Years Later: The Sequence, Structure and Function of Lacewing Cross-Beta Silk. *J. Struct. Biol.* **2009**, *168*, 467−475.
(44) Serpell, L. C. Alzheimer's amyloid fibrils: structure and assembly. *Biochim. Biophys. Acta, Mol. Basis Dis.* **2000**, *1502*, 16−30.
(45) Inouye, H.; Fraser, P. E.; Kirschner, D. A. Structure of β-Crystallite Assemblies Formed by Alzheimer beta-Amyloid Protein Analogues: Analysis by X-ray Diffraction. *Biophys. J.* **1993**, *64*, 502−519.
(46) Inouye, H.; Sharma, D.; Goux, W. J.; Kirschner, D. A. Structure of Core Domain of Fibril-Forming PHF/Tau Fragments. *Biophys. J.* **2006**, *90*, 1774−1789.
(47) Malinchik, S. B.; Inouye, H.; Szumowski, K. E.; Kirschner, D. A. Structural Analysis of Alzheimer's β(1−40) Amyloid: Protofilament Assembly of Tubular Fibrils. *Biophys. J.* **1998**, *74*, 537−545.
(48) Oster, G.; Riley, D. P. Scattering from Cylindrically Symmetric Systems. *Acta Crystallogr.* **1952**, *5*, 272−276.
(49) Klug, H. P.; Alexander, L. E. *X-ray Diffraction Procedures: For Polycrystalline and Amorphous Materials*, 2nd ed.; Wiley Interscience: New York, NY, USA, 1974.

DOI: 10.1021/acsami.5b06219
ACS Appl. Mater. Interfaces 2015, 7, 20875−20884

(50) Duka, V.; Czaplewsky, C.; Segalen, V.; Liepina, I. Molecular Modeling of Single Beta-Sheet and the Beta-Sheet Stack of Amyloid Protein 25−35. *Mater. Sci. Appl. Chem.* **2011**, *23*, 62−72.
(51) Riekel, C.; Di Cola, E.; Reynolds, M.; Burghammer, M.; Rosenthal, M.; Doblas, D.; Ivanov, D. A. Thermal Transformations of Self-assembled Gold Glyconanoparticles Probed by Combined Nanocalorimetry and X-ray Nanobeam Scattering. *Langmuir* **2015**, *31*, 529−534.
(52) Marinaro, G.; Accardo, A.; Benseny-Cases, N.; Burghammer, M.; Castillo-Michel, H.; Cotte, M.; Dante, S.; De Angelis, F.; Di Cola, E.; Di Fabrizio, E.; Hauser, C.; Riekel, C. Probing Droplets with Biological Colloidal Suspensions on Smart Surfaces by Synchrotron Radiation Micro- and Nano-Beams. *Opt. Lasers Eng.* **2015**, DOI: 10.1016/j.optlaseng.2015.03.004.
(53) Alsteens, D.; Ramsook, C. B.; Lipke, P. N.; Dufrêne, Y. F. Unzipping a Functional Microbial Amyloid. *ACS Nano* **2012**, *6*, 7703−7711.
(54) Peralta, M. D. R.; Karsai, A.; Ngo, A.; Sierra, C.; Fong, K. T.; Hayre, N. R.; Mirzaee, N.; Ravikumar, K. M.; Kluber, A. J.; Chen, X.; Liu, G.; Toney, M. D.; Singh, R. R.; Cox, D. L. Engineering Amyloid Fibrils from β-Solenoid Proteins for Biomaterials Applications. *ACS Nano* **2015**, *9*, 449−463.
(55) Varongchayakul, N.; Johnson, S.; Quabili, T.; Cappello, J.; Ghandehari, H.; Solares, S. D. J.; Hwang, W.; Seog, J. Direct Observation of Amyloid Nucleation under Nanomechanical Stretching. *ACS Nano* **2013**, *7*, 7734−7743.
(56) Yang, H.; Fung, S. Y.; Pritzker, M.; Chen, P. Surface-assisted Assembly of an Ionic-complementary Peptide: Controllable Growth of Nanofibers. *J. Am. Chem. Soc.* **2007**, *129*, 12200−12210.

DOI: 10.1021/acsami.5b06219
ACS Appl. Mater. Interfaces 2015, 7, 20875−20884